J Mater Sci (2010) 45:6707–6718
DOI 10.1007/s10853-010-4764-1

Microstructural stability of copper with antimony dopants at grain boundaries: experiments and molecular dynamics simulations

Rahul K. Rajgarhia · Ashok Saxena · Douglas E. Spearot · K. Ted Hartwig · Karren L. More · Edward A. Kenik · Harry Meyer

Received: 17 March 2010 / Accepted: 10 July 2010 / Published online: 24 July 2010
© Springer Science+Business Media, LLC 2010

Abstract This study presents evidence that the microstructural stability of fine-grained and nanocrystalline Cu is improved by alloying with Sb. Experimentally, $Cu_{100-x}Sb_x$ alloys are cast in three compositions (Cu-0.0, 0.2, and 0.5 at.%Sb) and extruded into fine-grained form (with average grain diameter of 350 nm) by equal channel angular extrusion. Alloying the Cu specimens with Sb causes an increase in the temperature associated with microstructural evolution to 400 °C, compared to 250 °C for pure Cu. This is verified by measurements of microhardness, ultimate tensile strength, and grain size using transmission electron microscopy. Complementary molecular dynamics (MD) simulations are performed on nanocrystalline Cu–Sb alloy models (with average grain diameter of 10 nm). MD simulations show fundamentally that Sb atoms placed at random sites along the grain boundaries can stabilize the nanocrystalline Cu microstructure during an accelerated annealing process.

R. K. Rajgarhia · A. Saxena · D. E. Spearot (✉)
Department of Mechanical Engineering, University of Arkansas, Fayetteville, AR, USA
e-mail: dspearot@uark.edu

K. T. Hartwig
Department of Mechanical Engineering, Texas A&M University, College Station, TX, USA

K. L. More · E. A. Kenik · H. Meyer
Oak Ridge National Laboratory, Oak Ridge, TN, USA

R. K. Rajgarhia
Cardiology, Rhythm and Vascular Division, Boston Scientific, St. Paul, MN, USA

Introduction

Although fine-grained (FG) and nanocrystalline (NC) materials have superior strength as compared to their coarse-grained counterparts [1–3], the excess enthalpy associated with the high volume fraction of grain boundaries [4] lowers the activation energy for grain growth [5] leading to premature and often abnormal grain growth at temperature and stress levels characteristic of many important engineering applications [6–9]. Studies focused on grain growth in NC materials using experiments [10–12] and simulations [13, 14] have demonstrated that the unusual grain growth occurs by elimination of unstable grain boundaries and is accompanied by a combination of several other mechanisms: grain boundary migration, grain boundary sliding, grain rotation, and emission of dislocations and twins from grain boundaries. The migration of grain boundaries is enhanced due to the high diffusivity of grain boundary atoms in NC materials. Natter et al. [15] conducted in situ X-ray diffraction (XRD) experiments of annealing in NC Fe with a grain size of 50 nm and showed that the activation energy for grain growth from 50 to 100 nm is equal to the activation energy for diffusion of grain boundary atoms. They also measured the activation energy for grain growth in FG Fe from 100 to 200 nm and found it to be equal to the activation energy for self diffusion of grain boundaries, indicating a change in the mechanism for grain growth as a function of grain size. Although grain growth in fine-grained and nanocrystalline materials has been studied for several decades, a complete understanding of the limiting mechanisms for grain growth has not been established.

It has been proposed that premature grain growth can be suppressed by reducing the amount of high energy boundaries [16] or through the addition of dopant atoms at

the grain boundaries [17–20]. In the thermodynamic model proposed by Kirchheim [18], the addition of dopants nullifies the grain boundary energy (excess enthalpy), which allows the microstructure to attain a metastable equilibrium state. Millett et al. [19, 20] conducted a parametric study using molecular dynamics (MD) simulations and showed that the addition of dopants can improve microstructural stability and that the concentration of dopants needed to reduce the grain boundary energy to zero, for a particular average grain size, depends strongly on the ratio of the radius of the dopant and host atoms (R_{dopant}/R_{host}). Other researchers have proposed that along with the reduction in the grain boundary energy, dopants improve microstructural stability by altering grain boundary kinetics, leading to "grain boundary pinning" or "solute-drag" effects. By altering the grain boundary kinetics, dopants at the grain boundaries increase the activation energy for diffusion of grain boundary atoms, thereby reducing grain boundary mobility and inhibiting grain growth [8, 21, 22]. Recently, Chen et al. [23] and Li et al. [24] demonstrated that the thermodynamic effect of reduction in grain boundary energy plays a bigger role than the kinetic solute-drag effect in microstructure stabilization.

Although placement of dopants at the grain boundaries seems like a promising approach, it is important to note that dopant atoms will be ineffective in stabilizing the microstructure if they are soluble in the host grains or form precipitates (at a specific local composition and temperature) with the host atoms [18], posing a severe limitation on material selection. For example, MD studies of NC nickel doped with tungsten showed that the grain boundary energy cannot be driven to zero for any tungsten composition at the grain boundaries [25]. This is probably because the solubility of W in Ni is significant (12 at.% at room temperature). The selection method for a dopant species suitable for a particular host matrix to improve microstructural stability is not well established in the literature. Improper selection of the dopant species can require large dopant concentrations to stabilize the microstructure and lead to the formation of precipitates which can negatively impact the functional properties of the material. For example, Botcharova et al. [26] showed that although Nb dopants (10 at.%) can be used to produce NC Cu stable up to 900 °C, the high processing temperatures caused the formation of large precipitates which resulted in a 90% reduction in electrical conductivity.

Many researchers have previously used dopants (cf. $Au_{100-x}Cu_x$, $Au_{100-x-y}Cu_x$–Sn_y [27], Cu-0.2 wt%B [28], $Cu_{100-x}Nb_x$ [26], Ni-1.2 wt%P [29], $Fe_{100-x}Ag_x$ [30], $Fe_{100-x}Zr_x$ [31], $Pd_{100-x}Zr_x$ [32], RuAl-12 wt%Fe [33], $Y_{100-x}Fe_x$ [34]) to improve the stability of fine-grained or nanocrystalline materials. In these studies, alloys were prepared either by electron [27, 29] or laser [30] deposition, or by compaction of powders processed by mechanical alloying [26, 28, 31–33] or inert gas condensation [34]. These studies showed that stability of NC materials can be improved by adding dopants; however, the quantities of material produced from these techniques are not sufficient for conducting mechanical tests as per ASTM standards which is necessary to provide an understanding of the effect of dopant atoms on the mechanical properties of the host material.

This study shows that the microstructural stability of Cu is improved by alloying with Sb without negatively affecting mechanical strength. This study focuses specifically on dilute amounts of Sb in Cu, with experimental compositions of 0.2 and 0.5 at.%Sb. The selection criterion for Sb as the dopant material in Cu is discussed. Experimentally, the $Cu_{100-x}Sb_x$ alloys are processed into fine-grained form using an equal channel angular extrusion (ECAE) method. Using ECAE, fully dense alloys can be produced economically, rapidly, and in large enough quantities to machine specimens for mechanical testing as per ASTM standards [35]. Microstructural stability analysis using tensile tests, microhardness tests, and transmission electron microscopy (TEM) shows that the Sb-doped fine-grained alloys have improved stability when compared to pure Cu. Analysis of the fine-grained microstructure and fracture surfaces suggests that the improved microstructural stability is due to the segregation of Sb to the grain boundaries. To complement experiments, MD simulations of grain growth in nanocrystalline $Cu_{100-x}Sb_x$ alloys are performed to study the influence of Sb on microstructural stability. These simulations are conducted for a range of Sb concentrations (0–0.5 at.%Sb) and elucidate connections between the reduction in excess grain boundary energy by Sb dopants and microstructural stability. It is found that Sb atoms placed at random grain boundary sites reduce the total excess energy in the NC model, but kinetic contributions are also present for the purposes of stabilizing the nanocrystalline microstructure, in agreement with concepts proposed by Chen et al. [23].

Material selection and processing

Material selection

Copper is selected as the host material because it is face-centered cubic with good formability, known macroscale deformation characteristics, and has been shown to develop an average grain size in the range of 100–400 nm when subjected to ECAE [36]. In addition, there are well-developed interatomic potentials for Cu to be used in the MD simulations [37–39]. The experimental techniques to characterize the mechanical properties of Cu, both in

fine-grained and in nanocrystalline forms have been established [1]. Hence, Cu is an ideal model material to study microstructural evolution in FG and NC materials.

The selection of the dopant element and concentration is based mainly on three criteria: (i) the dopant atoms should not form precipitates or secondary phases at the chosen composition and temperature [18], (ii) the dopant atoms should segregate to the grain boundaries, and (iii) the dopant atom size should be larger than the host atom to be effective in inhibiting grain boundary sliding [40]. Antimony has limited solubility in copper at room temperature ($\sim$1.0 at.%Sb) [41] due to the mismatch in both atomic size and crystal structure. At equilibrium, the Cu–Sb system will not contain intermetallic secondary phases if the concentration of Sb is below the solvus limit. Furthermore, there is experimental verification that Sb almost completely segregates to the grain boundaries in Cu when heated to 675 °C [42]. Since an Sb atom is much larger than a Cu atom ($R_{Sb}/R_{Cu} = 1.25$ [43]), Sb atoms at the grain boundaries are hypothesized to be effective in stabilizing the microstructure through both kinetic and thermodynamic mechanisms. Thus, Sb satisfies all the major criteria as a dopant material to stabilize the microstructure of Cu and is selected in this work as the dopant for the Cu host material.

Rectangular billets of size 23 × 23 × 202 mm with Cu-0.2 and 0.5 at.%Sb concentrations are prepared at Oak Ridge National Laboratory by casting in an induction arc furnace under argon gas cover. Cu billets prepared by the same casting process and commercially pure Cu in wrought form (Cu-CDA102, 99.95 wt%Cu, oxygen-free) are included in this study to establish control data. The Cu-102 sample has been previously cold-worked (extruded); the impact of this history on hardness and strength is discussed in "Experimental results and discussion." The chemical compositions of the alloys prepared by casting are shown in Table 1. The chemical analysis results show that the Sb concentrations are within the practical error limit of the casting process, but oxygen has penetrated the billets during casting. Scanning electron microscopy (SEM) analysis of the cast microstructures reveals that oxygen is present in the form of oxide particles of diameter 2–5 μm and that a large fraction of the oxide particles are located at the grain boundaries; the impact of these oxide particles on grain growth will be discussed in "Experimental results and discussion." In the case of Sb-doped alloys, energy dispersive X-ray spectrometry (EDS) analysis shows that the oxide particle positions coincide with much of the Sb. SEM and EDS results for Cu-0.5 at.%Sb are shown in Fig. 1; similar results are obtained for Cu and Cu-0.2 at.%Sb. The segregation of the Sb atoms to the oxide particles is due to the limited solubility of Sb in Cu and a preference for interfaces such as those at oxide particles and grain boundaries. The grain size of the cast alloys is between 50 and 100 μm.

Table 1 Chemical composition of the $Cu_{100-x}Sb_x$ alloys prepared by casting in an induction arc melting furnace under an argon gas cover

Element	Alloys (cast)		
	Cu	0.2 at.%Sb	0.5 at.%Sb
Sb	–	0.229	0.634
O	2.44	0.637	0.593
C (ppm)	38	41	32.5
Cr, Fe, Mg, Mn, Ni, Si, Ti (ppm)	<10	<10	<10
Cu	Balance	Balance	Balance

The concentrations of Sb, C, and O represent averages from measurements on two billets

Equal channel angular extrusion

Techniques capable of producing FG or NC materials can be divided into two categories. Bottom-up approaches include electron deposition and compaction from powders created via inert-gas condensation [44] or ball milling [45]. Top-down techniques, such as the ECAE, commonly involve severe plastic deformation and are capable of producing larger quantities of FG and NC samples with low residual porosity and contamination, compared to bottom-up approaches. The smallest average grain size produced by ECAE to date is about 100 nm, depending on extrusion conditions and die geometry [46, 47]. The billets in this study are extruded using the ECAE "E" route where billets are passed through the die four times. According to the E route, the billets are rotated 180° after the first pass, 90° after the second pass, and finally 180° after the third pass. Initially, billets were extruded at ambient temperature. However, the cast billets (Cu, Cu-0.2 at.%Sb, and Cu-0.5 at.%Sb) cracked and failed before the fourth pass. This is likely due to the presence of oxide particles which reduces the ductility of the cast billets; the oxygen-free Cu-102 samples were successfully extruded at ambient temperature through four passes. In order to extrude the cast billets without cracking, the extrusion temperature is increased.

To determine an appropriate higher extrusion temperature, 25.4 × 25.4 × 6.5 mm sections were cut from the cast Cu–Sb alloy billets and rolled to 95% reduction in thickness in five steps at room temperature. Although the cast billets failed during ECAE at room temperature, no cracking was observed after rolling, likely due to a difference in the stress states between the ECAE and the rolling processes. Sections from the rolled alloys were then annealed at selected temperatures between 200 and 600 °C

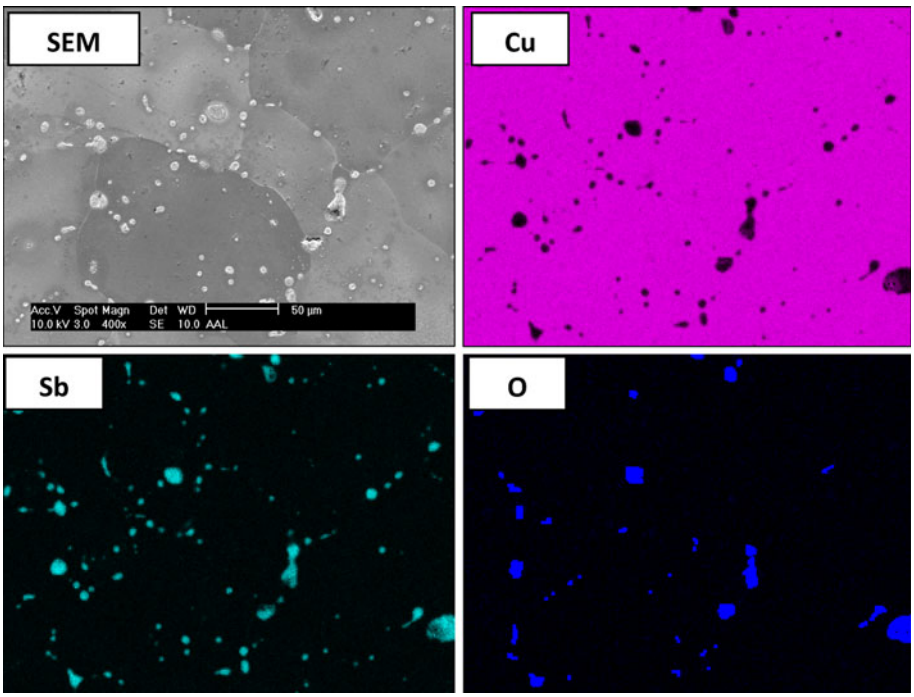

Fig. 1 SEM and EDS maps of Cu-0.5 at.%Sb alloy after casting (before ECAE)

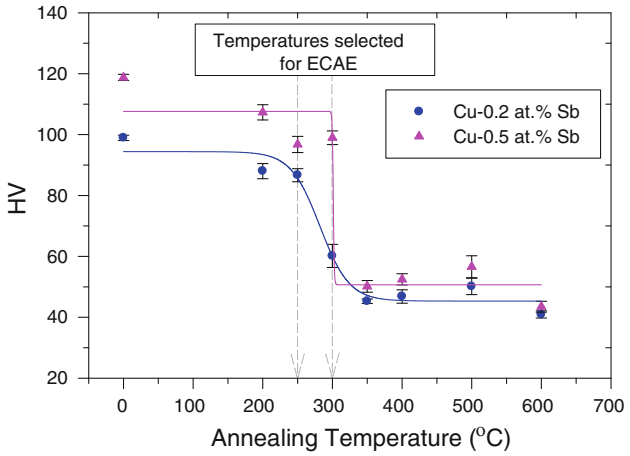

Fig. 2 Vickers microhardness (HV) measurements for cold-rolled Cu-0.2 and 0.5 at.%Sb samples after annealing for 1 h at each temperature. The indenter load used for all measurements is 0.01 kg. Each data point represents the average of four measurements and the error bars indicate ± standard error

for 1 h in a N_2 environment. Microhardness measurements on the annealed samples were performed and are plotted versus the annealing temperature in Fig. 2. The microhardness shows a decrease after 250 °C, indicating coarsening begins beyond this annealing temperature for this microstructure. Thus, to impart maximum ductility and prevent grain growth during ECAE, extrusions of the cast billets are performed at 250 °C, below the temperature at which microstructural evolution occurs. With a punch speed of 0.42 mm/s (0.10 in/min), the cast billets were extruded successfully for all four passes except for some surface cracks, which appeared in the billets during the third pass. To further increase the ductility of the material, a second batch of cast billets was extruded at 300 °C with a lower punch speed of 0.22 mm/s (0.05 in/min). The billets extruded at 300 °C were completely crack-free. Note, prior to each extrusion pass, the billets were heated in a muffle furnace for 15 min at the extrusion temperature. The entire die assembly was also heated to the desired temperature prior to extrusion.

Experimental results and discussion

Thermal stability analysis using TEM and OIM

The cast billets extruded at 250 and 300 °C were used for the experimental analysis of microstructural stability and mechanical properties. The end portions of the billets processed using ECAE were not extruded completely, thus 25 mm was cut from the ends of each billet and discarded; the remaining billet section was used for testing and analysis. To quantify the effect of Sb dopants on the microstructural stability of Cu, grain size measurements using Abrams Circular Intercept Procedure in ASTM E112 were taken on the extruded alloys before and after annealing at 250 °C for 1 h. This annealing temperature was selected because one of the potential applications for nanocrystalline or fine-grained Cu is chip-substrate interconnects in integrated circuits [48] and it is critical that the microstructure remains stable at 250 °C to be suitable for this application [49]. Annealing was performed in a N_2

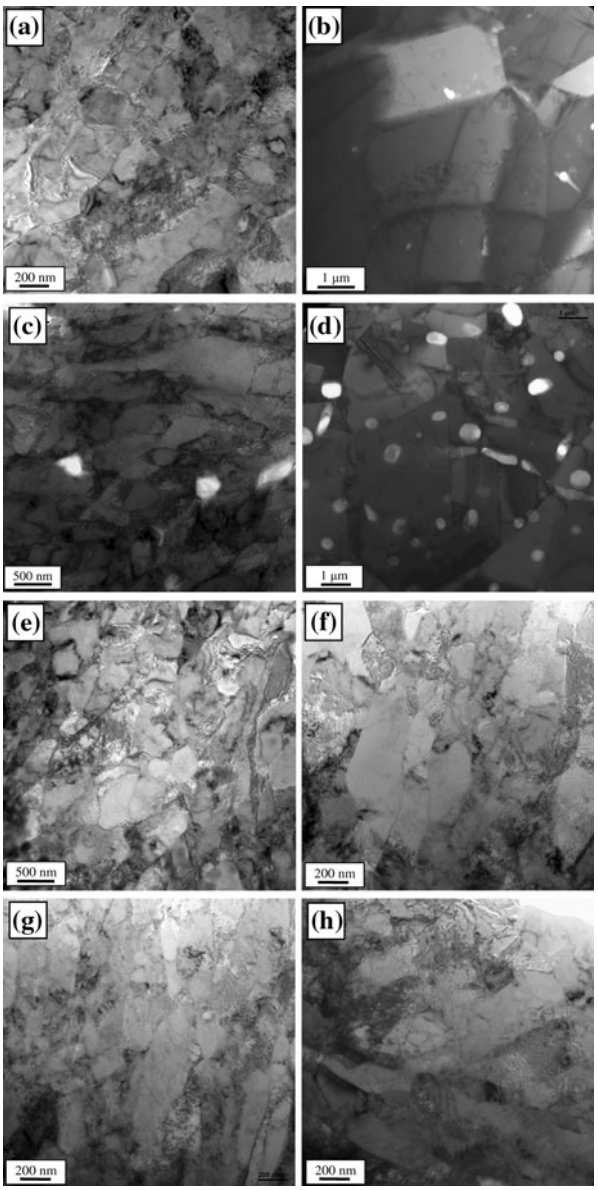

Fig. 3 TEM images of Cu-102 (**a**, **b**), Cu (**c**, **d**), Cu-0.2 at.%Sb (**e**, **f**), Cu-0.5 at.%Sb (**g**, **h**) in the extruded and annealed states. Figures in the *left column* (**a**, **c**, **e**, **g**) are of the extruded state and in the *right column* (**b**, **d**, **f**, **h**) are after annealing at 250 °C for 1 h

environment to avoid surface oxidation; the grain size was analyzed using TEM on samples prepared by electropolishing.

The TEM results in Fig. 3 indicate that the grain size after ECAE was approximately 350 nm with a narrow range (±5 nm) and high dislocation density. After annealing for 1 h at 250 °C, the microstructures of Cu and Cu-102 undergo grain growth resulting in a grain size of 2.05 and 2.11 μm, respectively. The TEM images show that the dislocation density decreases significantly after annealing in the Cu and Cu-102 specimens. However, after annealing for 1 h, the average grain size for the Sb-doped samples remains stable for Cu-0.2 and 0.5 at.%Sb, respectively, with some recovery providing a slight reduction in the dislocation density. The TEM results provide visual evidence that Sb atoms inhibit grain growth in Cu at 250 °C.

Orientation imaging microscopy (OIM) was conducted to study the distribution of grain boundary disorientations [50] in the $Cu_{100-x}Sb_x$ alloys after ECAE and to elucidate the influence of annealing on the grain boundary orientation distribution function. The OIM analysis shown in Fig. 4 reveals that each fine-grained sample has concentrated regions of small angle grain boundaries separated by large angle grain boundaries. One specific OIM result for ECAE processed Cu-0.2 at.%Sb is shown in Fig. 4a–d. Samples contain a high fraction of low-angle boundaries (<15° disorientation angle) which is shown in Fig. 4b and d. As a result of the somewhat arbitrary cutoff between low- and high-angle boundaries, some boundaries change category along their length as the misorientation between the adjacent grains varies in these deformed specimens. Similar results for grain boundary disorientation angle distribution functions are obtained for pure cast Cu. Dalla Torre et al. [36] studied the influence of the number of ECAE passes on the grain boundary misorientation distribution and also observed a similar large fraction of low-angle boundaries after four ECAE passes, the fraction of which decreased with increasing number of passes. The OIM results for the Cu-0.2 at.%Sb after annealing show that there is no change in the grain orientation distribution. However, the pure Cu fine-grained sample undergoes grain growth (Fig. 3b) and the microstructure is completely altered after annealing. These results further verify that along with the grain size, the Sb doping is able to retain the grain orientation distribution in Cu thereby preventing any changes in the properties associated with material texture.

Thermal stability analysis using microhardness and tensile tests

To evaluate the effect of Sb dopants on the temperature associated with microstructural evolution in fine-grained Cu, microhardness tests are conducted for ECAE processed alloys that are annealed at temperatures between 50 and 700 °C for 1 h at intervals of 50 °C in a N_2 environment. The effect of the annealing temperature on microhardness, for the alloys extruded at 250 °C, is shown in Fig. 5. It is clear from Fig. 5 that microhardness decreases sharply between 200 and 250 °C for the Cu-102 and cast Cu materials, indicating that grain growth has begun, whereas the Sb-doped Cu alloys retain their microhardness up to approximately 400 °C. Beyond 400 °C, the microhardness of each cast material decreases and plateaus at a value similar to that of the samples before ECAE. The annealed

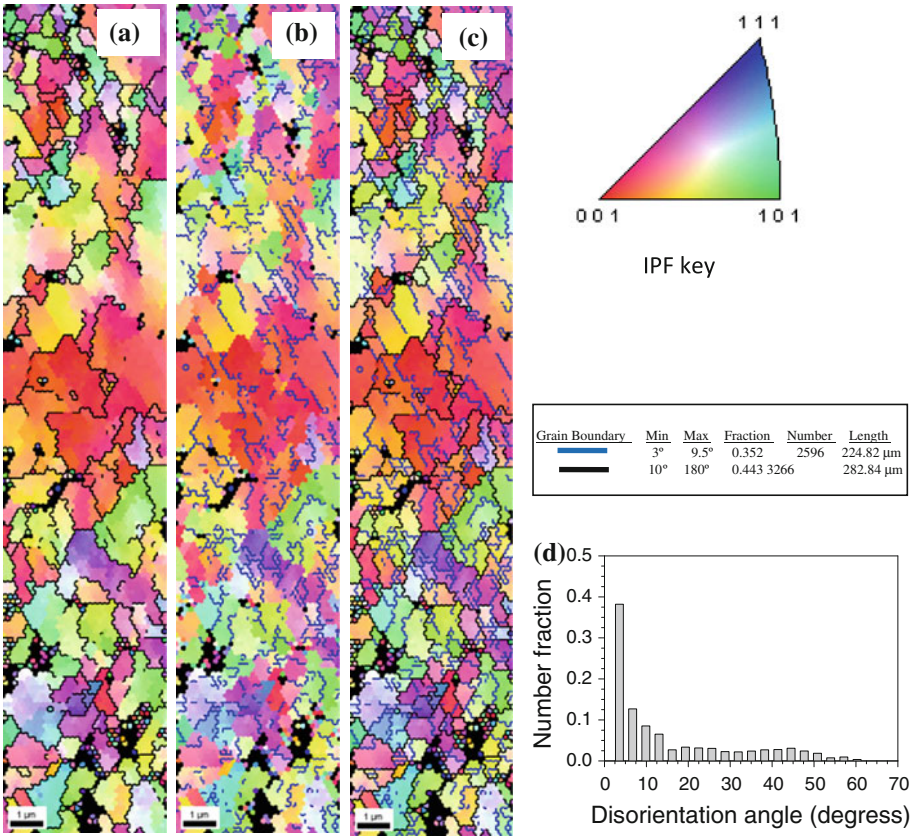

Fig. 4 Inverse pole figures (IPF) of nanocrystalline Cu-0.2 at.%Sb showing the high-angle boundaries (**a**), low-angle boundaries (**b**), and the low- and high-angle boundaries in the same image (**c**). Grains are colored by the orientation of their normal to the surface, corresponding to the IPF key. The grain boundary disorientation distribution is shown in (**d**)

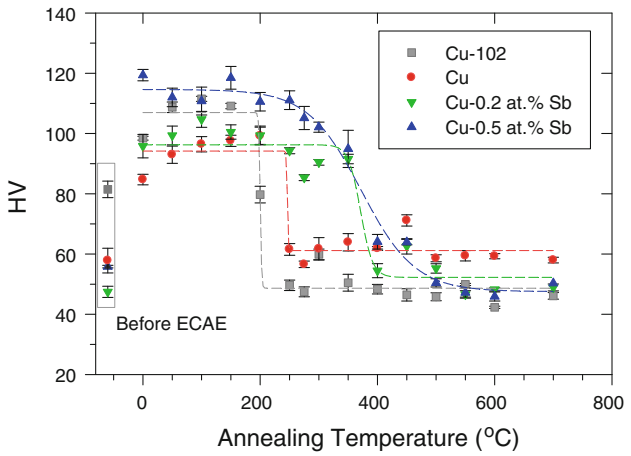

Fig. 5 Effect of annealing temperature on the Vickers microhardness (HV) of Cu samples and $Cu_{100-x}Sb_x$ alloys. The $Cu_{100-x}Sb_x$ alloys are extruded at 250 °C and Cu-102 is extruded at ambient temperature. Each data point represents the average of four measurements and the error bars indicate ±standard error

hardness of the Cu-102 sample is less than that prior to ECAE because the previous cold-work is removed by the annealing process. Similar results are obtained for the $Cu_{100-x}Sb_x$ alloys extruded at 300 °C, where the Sb-doped Cu material retains its microhardness at a higher temperature as compared to pure (undoped) Cu.

In addition to the microhardness study, the effect of annealing temperature on ultimate tensile strength is analyzed for the $Cu_{100-x}Sb_x$ alloys extruded at 300 °C and the Cu-102 sample. For efficient utilization of material and lower machining costs compared to round specimens, small flat dog-bone-type specimens of gauge length 8.2 mm, width 3 mm, and thickness 1 mm are utilized for the tensile tests. The test specimens are annealed in a N_2 environment over a range of temperatures (0–450 °C) before testing. The ultimate tensile strength (UTS) for each sample is reported in Fig. 6; observations are similar to the microhardness results in Fig. 5. Specifically, the tensile test results show that the strength of the pure Cu samples (cast Cu and Cu-102) decreases for annealing temperatures of 200 °C or higher, indicating microstructural coarsening, whereas the 0.5 at.%Sb-doped Cu alloy retains its strength up to 350 °C.

In summary, Sb-doped Cu alloy specimens retain their mechanical strength up to a higher annealing temperature as compared with Sb-free Cu samples. Furthermore, since grain growth is observed in Sb-free cast Cu at annealing temperatures greater than 250 °C, oxygen impurities do not appear to assist in improving the stability of the host material; the improvement in the stability can be attributed primarily to the presence of Sb dopants.

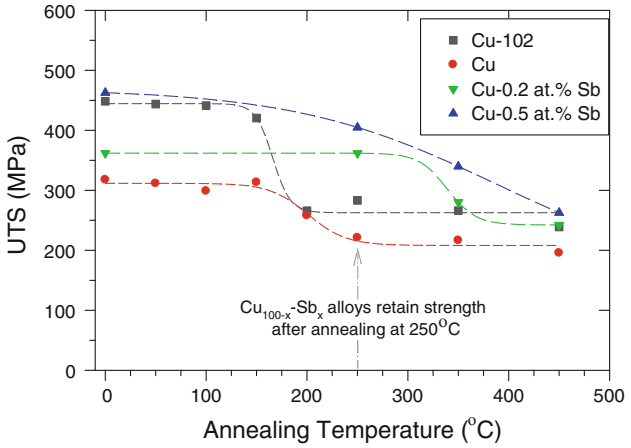

Fig. 6 Effect of annealing temperature on the ultimate tensile strength of $Cu_{100-x}Sb_x$ alloys and Cu samples. The $Cu_{100-x}Sb_x$ alloys are extruded at 300 °C and Cu-102 is extruded at ambient temperature. The samples are annealed for 1 h in a N_2 environment

Fracture surface analysis

SEM and Auger Electron Spectroscopy (AES) are used to investigate whether Sb atoms have segregated to the grain boundaries during casting or ECAE processing. The samples used for SEM and AES analyses are prepared from the cast alloys extruded into fine-grained form at 300 °C in the shape of a round bar with length 20 mm and diameter 3.2 mm. Specimens are fractured by striking a "knife" edge through each Cu–Sb sample at a high rate in an ultra high vacuum chamber followed immediately by analysis of the fracture surfaces. Figure 7a shows a SEM image of the fracture surface in a Cu-0.2 at.%Sb specimen. The SEM image in Fig. 7a shows the presence of ridges on the fracture surface with dimples that are approximately 5–20 μm in diameter in between the ridges. The ridges may indicate the positions of grain boundaries after casting (grain size 50–100 μm) while the dimples provide evidence that fracture is ductile. Figure 7b shows a higher-magnification image of a Cu-0.5 at.%Sb specimen, showing oxide particles in many of the dimples on the fracture surface. Recall, Fig. 1 shows that the majority of the oxide particles are located at the grain boundaries in the cast samples; thus, it is hypothesized that the ductile fracture mode is intergranular along the grain boundaries in the cast samples and that oxide particles act as nucleation sites for voids along the grain boundary planes.

Figure 8 shows the nonuniform distribution of Sb on the fracture surface in the Cu-0.2 at.%Sb sample; similar results are obtained for Cu-0.5 at.%Sb alloys. The elemental maps of O are very similar to those of Sb, analogous to that observed in the EDS maps of Sb and O in Fig. 1. The thickness of the Sb and O layers on the fracture surface is quantitatively measured by sputtering the fracture surface with Ar^+ ions. A region larger than the SEM image shown in Fig. 7b is sputtered, with data collected at a specific point within one of the dimples (e.g., point o1). The concentration profiles of Cu, Sb, and O as a function of the sputtering depth on the fracture surface of a Cu-0.5 at.%Sb sample are shown in Fig. 9. The Sb concentration on the fracture surface is quite high (4.5 at.%Sb), which is much greater than the measured average bulk concentration 0.634 at.%Sb (Table 1). Moreover, the concentration of Sb at the fracture surface is greater than the solid solubility of Sb in Cu at room temperature [41]; this suggests that fracture follows regions of high Sb concentration which Fig. 1 shows are at the grain boundaries after casting prior to ECAE. The concentration of Sb gradually decreases with increasing sputtering depth, and plateaus at a depth of 1.5 nm. The sputtering profile obtained for oxygen is similar to the profile of Sb. It is important to note that the O coverage on the fracture surface is also nonuniform and is not from contamination of the surface after the fracture, as evident from Fig. 8c (Table 2).

It is interesting to find that SEM analysis of the fracture surface shows evidence of ductile fracture while Ar^+ sputtering of the fracture surface returns Sb concentrations higher than those typically associated with Sb in Cu solid solution. The concentration of Sb on the fracture surface should promote very brittle behavior, similar to that shown

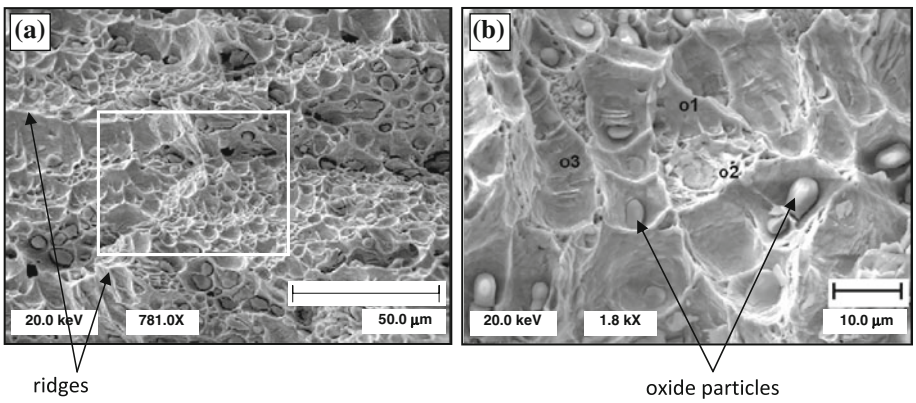

Fig. 7 **a** SEM image of the fracture surface in a Cu-0.2 at.%Sb specimen. The *white box* indicates the region over which AES scans are performed as shown in Fig. 8. **b** SEM image of fracture surface in a Cu-0.5 at.%Sb specimen. Points o1, o2, and o3 indicate where element composition analysis was performed with results presented in the Table 2

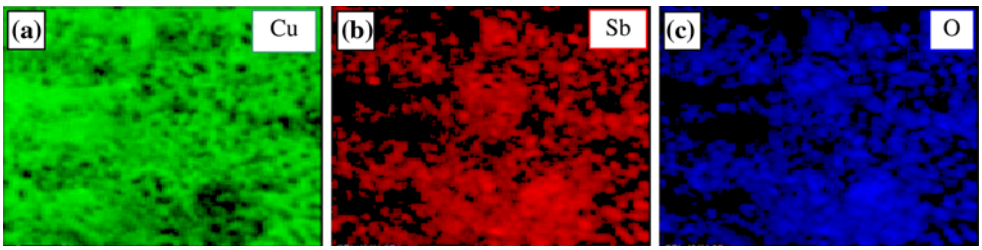

Fig. 8 AES element maps of the fracture surface in the Cu-0.2 at.%Sb alloy. The elemental maps are derived by analyzing the area inside the *white box* shown in Fig. 7**a**

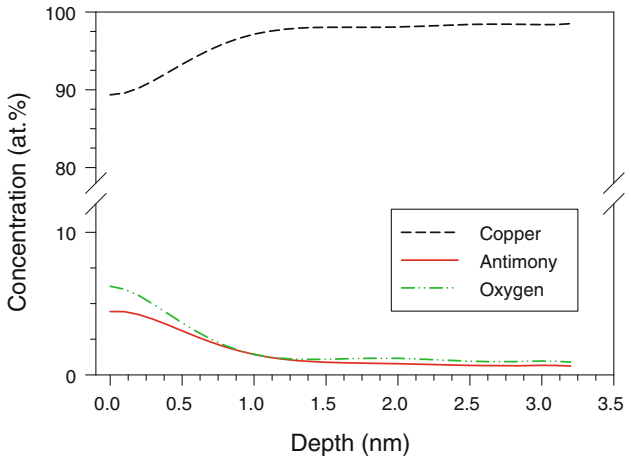

Fig. 9 Sputtering profile of fracture surface of nanocrystalline Cu-0.5 at.% Sb. The depth scale is determined using a calibrated sputter rate on a standard 100 nm SiO_2 film

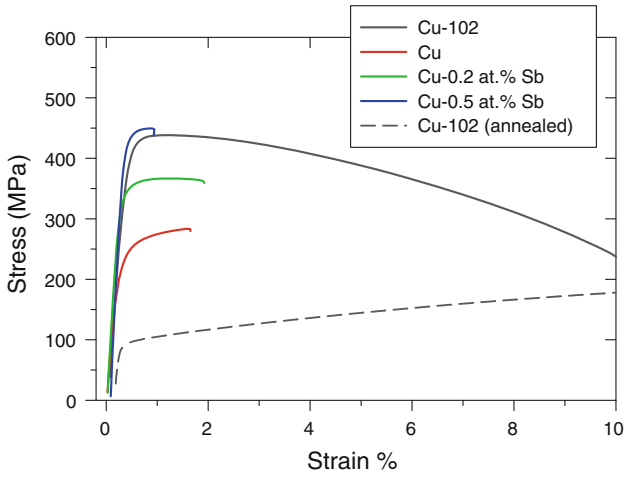

Fig. 10 Room temperature tensile tests of Cu and Cu–Sb alloys processed using ECAE. The cast alloys were extruded at 300 °C and Cu-102 was extruded at ambient temperature. The "Cu-102 (annealed)" sample is annealed at 500 °C for 2 h in a N_2 environment to return the sample to a coarse-grained microstructure. Note that the curves are slightly offset for clarity

Table 2 Elemental composition analysis at the points o1, o2, and o3 in Fig. 7b

Point	Composition (at.%)		
	O	Cu	Sb
o1	7.2	88.2	4.6
o2	54.3	4.9	40.8
o3	13.8	77.0	9.3

previously by Staley and Saxena [42]. There are two possible explanations for this behavior: (i) a disproportionate amount of the free Sb has segregated to the incoherent interfaces between the oxide particle and the Cu leaving the grain boundary regions, and/or (ii) the nanostructure created during ECAE is capable of absorbing some of the Sb from the original grain boundaries after casting lowering the effective concentration at each interface in the alloy. This provides an interesting direction for future research, to produce oxide-free $Cu_{100-x}Sb_x$ alloys with Sb, so that a more in depth analysis of Sb segregation can be performed in the absence of oxide particles.

Tensile strength and ductility of Cu-Sb alloys

Tensile tests are conducted at a strain rate of 0.001 s^{-1} in accordance with the ASTM E8 standard to study the influence of ECAE processing, extrusion temperature, and Sb concentration on the mechanical strength of $Cu_{100-x}Sb_x$ alloys. These tests are conducted at ambient temperature (~23 °C) using round tensile specimens with a gauge length and gauge diameter of 20 and 4 mm, respectively. Tensile test results for the cast alloys extruded at 300 °C and Cu-102 are shown in Fig. 10. The tensile test result for coarse-grained Cu-102, annealed at 500 °C for 2 h, is included in Fig. 10 to compare with the ECAE processed samples. Three important conclusions can be derived from the results presented in Fig. 10. (i) Comparing the tensile strength of the extruded and annealed Cu-102 sample, it is clear that processing the material using ECAE increases the yield strength of Cu from 92 to 435 MPa without a dramatic decrease in ductility. This is of course due to grain size strengthening. (ii) The presence of oxide impurities in

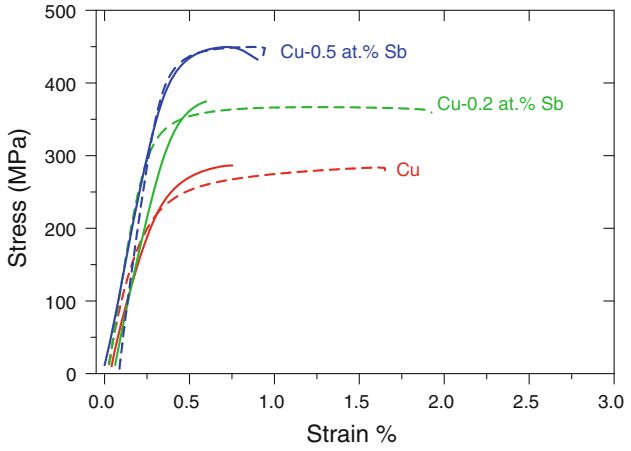

Fig. 11 Comparison of tensile properties of Cu_{100-x}–Sb_x cast alloys processed using ECAE at 250 °C (*solid line*) and 300 °C (*dashed line*). Note that the curves are slightly offset for clarity

Cu has a deleterious effect on ductility; Cu prepared by casting is significantly less ductile than that of Cu-102. The difference in strength between cast Cu and Cu-102 is primarily due to the cold-worked history of the Cu-102 specimen and the processing procedure as the Cu-102 sample was deformed via ECAE at ambient temperature, both of which will provide increased dislocation density compared to cast Cu. (iii) Comparing the tensile test results of the alloys prepared by casting only (Cu, Cu-0.2 at.%Sb, and Cu-0.5 at.%Sb) shows that the tensile strength increases with increasing Sb concentration. This behavior could be caused by solid solution strengthening and the fact that Sb atoms reduce the grain boundary energy, leading to increase in the stress required for sliding and nucleation of dislocations from the grain boundaries [40, 51]. Further, oxides in the Cu-0.2 and 0.5 at.%Sb samples contain Sb, whereas oxides in the cast Cu samples do not, which may contribute to the mechanical response.

Tensile tests are conducted on cast billets extruded at 250 °C are compared to the test results of the alloys extruded at 300 °C in Fig. 11. The Cu and Cu-0.2 at.%Sb alloys extruded at 300 °C have slightly lower yield strengths (approximately 15% reduction) but much improved ductility (300% increase) compared to the alloys extruded at 250 °C. There was no observable difference in the grain sizes of the alloys extruded at 250 and 300 °C, and the improvement in the ductility are likely caused by increased dislocation annihilation during ECAE at 300 °C as compared to 250 °C. However, there is no significant effect on the mechanical strength and ductility of the ECAE processing temperature for the Cu-0.5 at.%Sb alloy. In summary, the tensile test results demonstrate that there is no significant advantage of processing the billets at 250 °C over 300 °C. Recall that processing the billets at 250 °C resulted in cracking, whereas the billets processed at 300 °C were completely crack-free. It can therefore be concluded that it is more efficient to process the Cu_{100-x}–Sb_x billets at 300 °C compared to 250 °C.

Molecular dynamics simulation method

The fundamental role of Sb atoms at the grain boundaries on excess grain boundary energy and microstructural stability is analyzed using MD simulations. MD simulations are conducted using the code LAMMPS, developed by Plimpton et al. [52] at Sandia National Laboratories. The NC model is cubic with side lengths of 35 nm and contains over 3.5 million atoms. The Cu–Cu interaction is calculated using the EAM potential by Mishin et al. [37], while the Sb–Sb interactions and Cu–Sb interactions are calculated using a two-body Lennard–Jones (LJ) potential developed specifically to match the heat of solution and other structural aspects of dilute amounts of Sb in Cu [53] (this potential is not capable of modeling Cu–Sb alloys with higher Sb concentrations leading to intermetallic phase formation). The LJ parameters for Cu–Sb and Sb–Sb interactions used in this study are $\sigma_{Cu-Sb} = 2.744$ Å, $\varepsilon_{Cu-Sb} = 0.1798$ eV and $\sigma_{Sb-Sb} = 3.15$ Å, $\varepsilon_{Sb-Sb} = 0.079$ eV, respectively. The cut-off radius for the LJ potential is selected to be three times the value of σ_{Sb-Sb} (9.45 Å), which is approximately the radius of the strain field around an Sb atom in a Cu lattice [53]. The suitability and accuracy of these potentials have been discussed in previously by Spearot et al. [54, 55] and Rajgarhia et al. [53, 56].

The NC microstructure is constructed using the Voronoi tessellation method with a target grain size of 10 nm. With this grain size, direct comparison between the MD simulations and the experiments on FG Cu are not possible. Instead, the MD simulations provide an understanding of the underlying mechanisms of grain boundary stability in grain boundary-doped NC materials. The grain size distribution is constructed to be log-normal with random grain boundary disorientation distribution, in agreement with Mackenzie [57]. Further details of the construction method for the NC microstructure used in this study can be found in [58]. The Sb atoms are distributed randomly at the grain boundaries as substitutional defects by replacing Cu atoms at the grain boundaries with Sb atoms (using the centro-symmetry parameter [59] as a means to identify grain boundary atoms). At this time, no attempt is made to tailor the Sb concentration at each boundary as a function of grain boundary disorientation. The simulation cell is first subjected to energy minimization using a Polak–Ribière nonlinear conjugate gradient process. The NC model is then annealed at 1200 K at 0 bar in the isobaric–isothermal canonical ensemble [60, 61] for 1 ns, analogous to previous

calculations by Millett et al. [19, 20]. High temperature annealing is used simply to accelerate the grain growth process within the short-time scales characteristic of MD simulations. MD simulations are conducted for a range of Sb concentrations (0.0–2.0 at.%Sb) using identical initial NC microstructures.

MD simulation results and discussion

The influence of Sb concentration on excess grain boundary energy in nanocrystalline Cu is shown in Fig. 12. Grain boundary energy is computed at 0 K after the NC model is subjected to energy minimization. The excess grain boundary energy is computed as the difference between the total potential energy of the NC simulation model after energy minimization and an identical system with each atom considered to be in the bulk. The bulk energy of Cu is −3.54 eV/atom [37], and the bulk energy of Sb is approximated to be −2.207 eV/atom [53]. Grain boundary area is computed by summing the surface area of each grain assuming they are spheres with diameter equal to the average grain size, and then multiplying this by one-half to account for double counting, since two adjacent grains share a common grain boundary. Simulation shows that the excess grain boundary energy per unit grain boundary area, Γ, reduces with increasing Sb concentration. The zero value of Γ represents the concentration of Sb at which the thermodynamic driving force for grain growth is no longer present. These results are qualitatively consistent with grain boundary engineering concepts proposed previously by Weissmuller [17] and Kirchhiem [18].

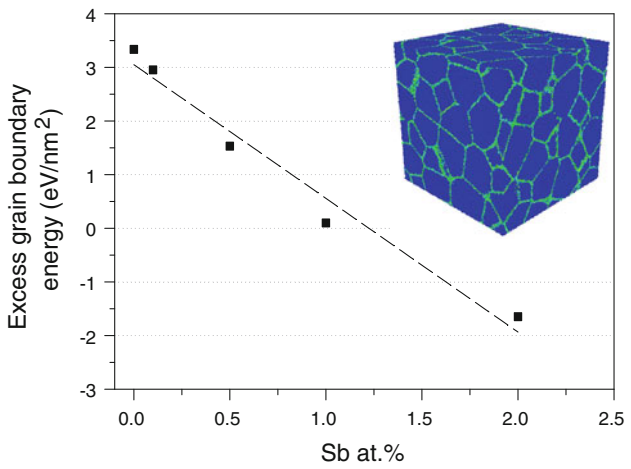

Fig. 12 MD simulation results showing the influence of Sb concentration on the excess grain boundary energy per unit grain boundary area (Γ). The average grain size of the microstructure used for this calculation is 20 nm. The *inset* image shows 3D nanocrystalline Voronoi model used for all calculations in this study

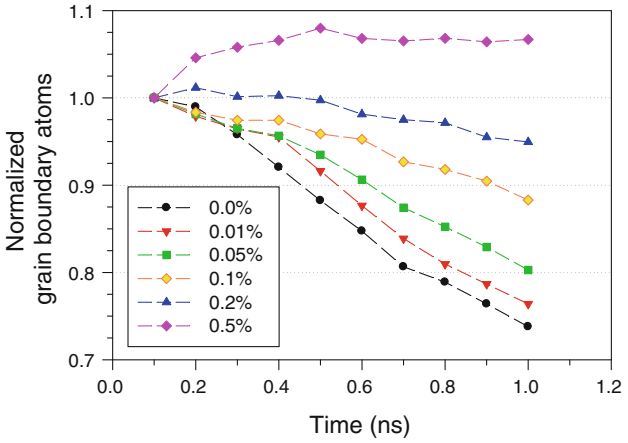

Fig. 13 MD simulation results showing change in number of grain boundary atoms (atoms with centrosymmetry > 0.5) during annealing at 1200 K for 1 ns for a range of Sb concentrations (0.0–0.5 at.%Sb). To ensure that the entire model is in equilibrium at 1200 K, the starting point for data collection is taken at 0.1 ns. Hence, the plotted values are normalized by the number of grain boundary atoms at 0.1 ns

Microstructural stabilization of NC Cu by Sb is examined in Figs. 13 and 14. The role of Sb dopants on microstructure stabilization is studied by two methods. First, the number of grain boundary atoms in the NC microstructure is tracked by counting the number of atoms with centrosymmetry >0.5 Å^2 over the annealing period, as shown in Fig. 13. For pure Cu, the number of grain boundary atoms clearly decreases signifying grain growth (visual inspection of the MD results confirms this observation). However, Sb atoms dispersed at the grain boundaries retard grain growth, leading to a stabilized NC Cu alloy microstructure for 0.2 at.%Sb and 0.5 at.%Sb with

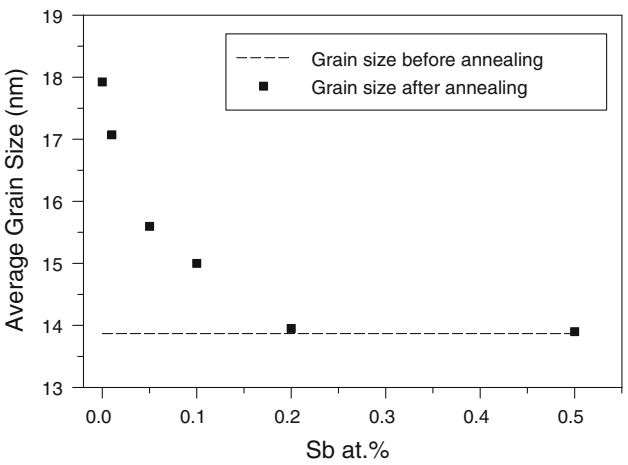

Fig. 14 MD simulation results showing the average grain size before and after annealing nanocrystalline Cu with different Sb concentrations. Grain size is calculated using the Abram's Three Circle Intercept method in ASTM E112

slight thickening of the distorted region around the grain boundaries observed in the latter case. Grain stability improves with increasing Sb concentration and becomes stable at 0.5 at.%Sb. The higher concentration of Sb causes greater distortion at the grain boundaries, which explains the increase in the number of atoms identified as belonging to the grain boundary after the 1 ns annealing.

Second, the average grain size is calculated at the end of the annealing period using the Abrams Three Circle Intercept method in ASTM E112 and compared with the grain size before annealing. The results of this comparison for a range of Sb concentrations are presented in Fig. 14. It is clear that grain stability increases with Sb concentration and that grain size remains stable during the simulation time for 0.2 and 0.5 at.%Sb concentrations. It is very important to note that although the excess grain boundary energy at concentration levels of 0.2 and 0.5 at.%Sb is not zero (Fig. 12), the combined kinetic and thermodynamic contributions are sufficient to maintain the grain stability at the conditions tested in this work. This implies that the excess grain boundary energy may not need to be zero to improve stability, and additional mechanisms such as grain boundary pinning and solute-drag at the grain boundaries are active and assist in providing microstructure stabilization.

Conclusions

Experiments conducted in this study show that the microstructural stability of fine-grained Cu (with average grain size of 350 nm) improves by alloying with Sb. Specifically, the temperature associated with microstructural evolution in Cu–Sb alloys (with 0.2 and 0.5 at.%Sb) is found to be approximately 400 °C as compared to 250 °C for pure Cu; this result is verified by measurements of grain size using TEM, microhardness, and ultimate tensile strength. In addition, the yield and ultimate tensile strengths of fine-grained Cu are found to increase with increasing Sb concentration. SEM images (Fig. 7) and chemical analysis (Figs. 8, 9) of fracture surfaces in Cu–Sb alloys show a ductile mode of fracture with high concentration of Sb (4.5 at.%) and oxide particles on the fracture surface. The presented results suggest that Sb dopants do segregate to the grain boundaries present after casting and that fracture is due to void nucleation and growth along these grain boundaries initiating at the oxide particles. Furthermore, it is hypothesized that a portion of the Sb concentration is absorbed at the incoherent interfaces between the oxide particles and/or at the new grain boundaries formed during ECAE, allowing for ductile rather than brittle fracture.

Molecular dynamics simulations on NC samples (with average grain diameter of 10 nm) show fundamentally that the addition of Sb at the grain boundaries lowers the excess free energy of the system, in agreement with previous theoretical predictions. However, it is clear that microstructure stabilization can be achieved through combined kinetic and thermodynamic mechanisms even if the excess grain boundary energy is not zero. Molecular dynamics simulations of accelerated annealing verify that the stability of the microstructure improves with increasing Sb concentration at the grain boundaries and that the microstructure is stable for 0.2 and 0.5 at.%Sb concentrations. The two methods used to study grain size during MD simulation of annealing in nanocrystalline $Cu_{100-x}Sb_x$ alloys are in close agreement.

This research shows that Sb is a suitable dopant for increasing the stability of the microstructure in Cu, as is has a tendency to segregate to internal interfaces (such as grain boundaries), lowers the excess grain boundary energy and has a positive effect on the mechanical strength. Using this approach, microstructural stability of fine-grained and nanocrystalline materials can be improved thereby enabling their use in elevated temperature engineering applications. In future work, creep deformation tests will be conducted to evaluate the effect of Sb dopants in fine-grained Cu under the combined influence of stress and temperature.

Acknowledgements Funding for this work was provided by the Irma and Raymond Giffels' Endowed Chair in Engineering at the University of Arkansas. DES appreciates additional support from Oak Ridge Associated Universities via the Ralph E. Powe Junior Faculty Enhancement Award. Molecular dynamics simulations were performed on "Star of Arkansas", funding for which was provided in part by the National Science Foundation under Grant MRI #072265. Support from the Department of Energy for conducting the TEM, OIM and Auger Spectroscopy analysis at the SHaRE User Facility at the Oak Ridge National Laboratory is acknowledged. TEM, OIM and Auger Electron Spectroscopy analysis were performed at the Oak Ridge National Laboratory SHaRE User Facility that is sponsored by the Division of Scientific User Facilities, Office of Basic Energy Sciences, U.S. Department of Energy. Support from the Texas Engineering Experiment Station for ECAE processing is gratefully acknowledged.

References

1. Dao M, Lu L, Asaro RJ, De Hosson JTM, Ma E (2007) Acta Mater 55:4041
2. Meyers MA, Mishra A, Benson DJ (2006) Prog Mater Sci 51:427
3. Weertman JR (1993) Hall-petch strengthening in nanocrystalline metals. Mater Sci Eng A 166:161
4. Gleiter H (2000) Acta Mater 48:1
5. Ganapathi SK, Owen DM, Chokshi AH (1991) Scripta Metall Mater 25:2699
6. Gunther B, Kumpmann A, Kunze HD (1992) Scripta Metall Mater 27:833
7. Gertsman VY, Birringer R (1994) Scripta Metall Mater 30:577
8. Rajgarhia RK, Koh SW, Spearot D, Saxena A (2008) Mol Simul 34:35
9. Moelle CH, Fecht HJ (1995) Nanostruct Mater 6:421

10. Zhang K, Weertman JR, Eastman JA (2005) Appl Phys Lett 87:61921
11. Hibbard GD, Radmilovic V, Aust KT, Erb U (2008) Mater Sci Eng A 494:232
12. Ames M, Markmann J, Karos R, Michels A, Tschope A, Birringer R (2008) Acta Mater 56:4255
13. Sansoz F, Dupont V (2006) Appl Phys Lett 89:111901
14. Farkas D, Froseth A, Van Swygenhoven H (2006) Scripta Mater 55:695
15. Natter H, Schmelzer M, Loffler MS, Krill CE, Fitch A, Hempelmann R (2000) J Phys Chem B 104:2467
16. Li JCM (2006) Phys Rev Lett 96:215506
17. Weissmuller J (1994) J Mater Res 9:4
18. Kirchheim R (2002) Acta Mater 50:413
19. Millett PC, Selvam RP, Saxena A (2007) Acta Mater 55:2329
20. Millett PC, Selvam RP, Saxena A (2006) Acta Mater 54:297
21. Michels A, Krill CE, Ehrhardt H, Birringer R, Wu DT (1999) Acta Mater 47:2143
22. Randle V (1996) The role of the coincidence site lattice in grain boundary engineering. Institute of Materials, London
23. Chen Z, Liu F, Wang HF, Yang W, Yang GC, Zhou YH (2009) Acta Mater 57:1466
24. Li J, Wang J, Yang G (2009) Scripta Mater 60:945
25. Detor AJ, Schuh CA (2007) Acta Mater 55:4221
26. Botcharova E, Freudenberger J, Schultz L (2006) Acta Mater 54:3333
27. Wang YM, Jankowski AF, Hamza AV (2007) Scripta Mater 57:301
28. Suryanarayanan R, Frey CA, Sastry SML, Waller BE, Buhro WE (1999) Mater Sci Eng A 264:210
29. Mehta SC, Smith DA, Erb U (1995) Mater Sci Eng A A204:227
30. Liu F, Chen Z, Yang W, Yang CL, Wang HF, Yang GC (2007) Mater Sci Eng A 457:13
31. Darling KA, Chan RN, Wong PZ, Semones JE, Scattergood RO, Koch CC (2008) Scripta Mater 59:530
32. Krill CE, Klein R, Janes S, Birringer R (1995) Mater Sci Forum 179–181:443
33. Liu KW, Mucklich F (2001) Acta Mater 49:395
34. Weissmuller J, Krauss W, Haubold T, Birringer R, Gleiter H (1992) Nanostruct Mater 1:439
35. Valiev RZ, Islamgaliev RK, Alexandrov IV (2000) Prog Mater Sci 45:103
36. Dalla Torre FH, Gazder AA, Pereloma EV, Davies CHJ (2007) J Mater Sci 42:1622. doi:10.1007/s10853-006-1283-1
37. Mishin Y, Mehl MJ, Papaconstantopoulos DA, Voter AF, Kress JD (2001) Phys Rev B 63:224101
38. Zimmerman JA, Gao H, Abraham FF (2000) Model Simul Mater Sci Eng 8:103
39. Van Swygenhoven H, Derlet PM, Froseth AG (2004) Nat Mater 3:399
40. Millett PC, Selvam RP, Saxena A (2006) Mater Sci Eng A 431:92
41. Subramanian PR, Chakrabarti DJ, Laughlin DE, Massalshi TB (1993) Phase diagrams of binary copper alloys. ASM International, Materials Park
42. Staley JT Jr, Saxena A (1990) Acta Metall 38:897
43. Schaffer J, Saxena A, Sanders T, Antolovich S, Warner S (2000) Science and design of engineering materials, 2nd edn. McGraw-Hill Science, New York
44. Haas V, Gleiter H, Birringer R (1993) Scripta Metall Mater 28:721
45. Koch CC (1993) Nanostruct Mater 2:109
46. Beyerlein IJ, Toth LS, Tome CN, Suwas S (2007) Philos Mag 87:885
47. Xue Q, Beyerlein IJ, Alexander DJ, Gray Iii GT (2007) Acta Mater 55:655
48. Aggarwal AO, Markondeya Raj P, Pratap RJ, Saxena A, Tummala RR (2002) Design and fabrication of high aspect ratio fine pitch interconnects for wafer level packaging. In: Proceedings 4th electronics packaging technology conference (EPTC 2002)
49. Bansal S, Saxena A, Tummala RR (2004) Nanocrystalline copper and nickel as ultra high-density chip-to-package interconnections. In: Proceedings—electronic components and technology conference
50. Randle V, Engler O (2000) Introduction to textru analysis: macrotexture, microtexture and orientation mapping. Gordon and Breach Science Publishers, London
51. Rajgarhia R, Spearot DE, Saxena A (2010) J Mater Res 25:411
52. Plimpton SJ, Large-scale atomic/molecular massively parallel simulator, http://lammps.sandia.gov
53. Rajgarhia R, Spearot DE, Saxena A (2008) Comput Mater Sci 44:1258
54. Spearot DE, Jacob KI, McDowell DL (2005) Acta Mater 53:3579
55. Spearot DE, McDowell DL (2009) J Eng Mater Technol 131:041204
56. Rajgarhia RK, Spearot DE, Saxena A (2009) Model Simul Mater Sci Eng 17:055001
57. Mackenzie JK (1958) Biometrika 45:229
58. Froseth AG, Van Swygenhoven H, Derlet PM (2005) Acta Mater 53:4847
59. Kelchner CL, Plimpton SJ, Hamilton JC (1998) Phys Rev B 58:11085
60. Hoover WG (1985) Phys Rev A 31:1695
61. Melchionna S, Ciccotti G, Holian BL (1993) Mol Phys 78:533